

TOWARDS PLANETESIMALS: DENSE CHONDRULE CLUMPS IN THE PROTOPLANETARY NEBULA

JEFFREY N. CUZZI^{1,4}, ROBERT C. HOGAN², AND KARIM SHARIFF³

Astrophys. J., Accepted, April 11 2008

ABSTRACT

We outline a scenario which traces a direct path from freely-floating nebula particles to the first 10-100km-sized bodies in the terrestrial planet region, producing planetesimals which have properties matching those of primitive meteorite parent bodies. We call this *primary accretion*. The scenario draws on elements of previous work, and introduces a new critical threshold for planetesimal formation. We presume the nebula to be weakly turbulent, which leads to dense concentrations of aerodynamically size-sorted particles having properties like those observed in chondrites. The fractional volume of the nebula occupied by these dense zones or clumps obeys a probability distribution as a function of their density, and the densest concentrations have particle mass density 100 times that of the gas. However, even these densest clumps are prevented by gas pressure from undergoing gravitational instability in the traditional sense (on a dynamical timescale). While in this state of arrested development, they are susceptible to disruption by the ram pressure of the differentially orbiting nebula gas. However, self-gravity can preserve sufficiently large and dense clumps from ram pressure disruption, allowing their entrained particles to sediment gently but inexorably towards their centers, producing 10-100 km “sandpile” planetesimals. Localized radial pressure fluctuations in the nebula, and interactions between differentially moving dense clumps, will also play a role that must be allowed for in future studies. The scenario is readily extended from meteorite parent bodies to primary accretion throughout the solar system.

Subject headings: solar system:formation; accretion disks; minor planets: asteroids; turbulence; instabilities

1. INTRODUCTION

There is no currently accepted scenario for the formation of the parent bodies of primitive meteorites which accounts for the most obvious of their properties. These properties (reviewed by Scott and Krot 2005 and discussed in more detail in section 2.1) include (a) dominance by aerodynamically well-sorted mineral particles of sub-mm size; (b) class-to-class variation in well-defined physical, chemical, and isotopic properties; (c) a spread of 1 Myr or so between the formation times of the oldest and youngest objects found in the same meteorite; (d) a spread of 1-3 Myr in radiometric ages of different meteorite types; and (e) a dearth of melted asteroids, with model results for even some melted asteroids which imply Myr delays in formation relative to ancient minerals. In recent years, meteoritic evidence has appeared for some very early-formed planetesimals, which represent a minority of both meteorites and asteroids. This implies that primary accretion started early and continued for several million years - thus, it was fairly inefficient and did not run quickly to completion.

Most current models for this “primary accretion” stage (reviewed by Cuzzi and Weidenschilling 2006 and Dominik et al 2007) can be classified as either (a) incremental growth, where large particles sweep up smaller ones by inelastic collisions involving porous surfaces, and

growth proceeds hierarchically; or (b) instability, where physical sticking is irrelevant and collective effects drive collapse to km-sizes or larger on very short timescales. Those who favor instability models, most of which rely on gravity and occur in a particle-rich nebula midplane, are concerned by the poorly understood sticking of mineral particle aggregates and the apparent difficulty of growing beyond meter size due to rapid inward migration and collisional disruption. Those who favor incremental growth have noted that midplane instability models are precluded by even very weak global turbulence, and that, in the dense midplane layers that form when turbulence is absent, incremental accretion is at low relative velocity and the meter-size barrier is not a problem. However, the most sophisticated models of incremental accretion in nonturbulent nebulae find it to be *so* efficient that large planetesimals grow in only $10^4 - 10^5$ years throughout the asteroid belt region (Weidenschilling 2000), a short time which is difficult to reconcile with constraints (a-e) above. A third class of scenario suggests that a complex interplay between several nonlinear processes - turbulence, pressure gradients, and gravity - may concentrate appropriately sized particles and lead to planetesimal growth (Cuzzi et al 2001, 2005, 2007; Johansen et al 2006, 2007). Scenarios which involve preferentially meter-sized objects encounter concerns about whether meter-sized objects can survive their own high-velocity mutual collisions in this sort of turbulent environment (*cf.* Sirono 2000, Langkowski et al 2007, Ormel et al 2007). However, in principle, such boulder-concentration scenarios can proceed independently in the same environment as discussed in this paper, where we focus on mm-size particles.

¹ Space Science Division, Ames Research Center, Moffett Field, CA 94035, USA

² BAER inc., Sonoma, CA

³ NASA Advanced Supercomputing Division, Ames Research Center

⁴ To whom correspondence should be addressed; E-mail: jeffrey.cuzzi@nasa.gov

Most of the above scenarios provide no natural explanation for observed meteorite properties (a) and (b) above. In particular, the evidence for the H chondrite class (and perhaps all the ordinary chondrites) suggests that entire asteroids of 10-100km diameter formed directly from a physically, chemically, and isotopically homogeneous mix of dust-rimmed particles of similar size (section 2.1). In this paper, we outline a possible path by which entire batches of mm-size, aerodynamically sorted particles might proceed directly in turbulence (even if sporadically) to planetesimals having the properties outlined above. We find that sufficiently large and dense clumps of mm-size particles can form by turbulent concentration such that, even if classical gravitational instability can't operate, their self-gravity may still allow them to survive disruptive forces and slowly sediment into a "sandpile" planetesimal. This simple analytical model is backed up by some numerical simulations that support the basic idea. In sections 2.2 and 2.3, we review the most relevant physics that determines the properties of dense, particle-rich zones or clumps in turbulent nebulae. In section 3, we address the fate of these dense clumps using analytical and numerical models of their evolution. We derive the combination of size and mass density a clump must have to evolve into a "sandpile" having some degree of internal strength. In subsequent stages not modeled here, we imagine that collisions and thermal sintering transform these sandpiles into the cohesive rocky parent bodies we see today. However, in the outer solar system, lower energy collisions and weaker thermal processing might well allow planetesimals to retain their initial low-strength states, as seen for some cometary objects (*eg.*, Asphaug and Benz 1996).

2. BACKGROUND

2.1. Meteoritics background and evidence for inefficient accretion in a turbulent environment

One can extract a number of clues from primitive (unmelted) meteorites regarding the primary accretion process by which their parent bodies first formed (Scott and Krot 2005, Taylor 2005). For the best evidence, one must look back through extensive subsequent evolutionary stages. Even unmelted bodies in the 100km size range have incurred extensive collisional evolution (Bischoff et al. 2006), producing compaction, fragmentation, and physical grinding and mixing on and beneath their surfaces, which may obscure the record of primary accretion. Model studies (*eg.*, Petit et al 2001, Kenyon and Bromley 2004, 2006; Bottke et al 2005; Chambers 2004, 2006; Weidenschilling and Cuzzi 2006) suggest that the collisional stage occurred after dispersal of the nebula gas allowed the orbital eccentricities of primitive bodies to grow. We are concerned with an earlier stage, when the still-abundant nebula gas led to a more benign environment with fewer and gentler collisions. The direct products of primary accretion might be most clearly visible in the rare "primary texture" seen in some CM (Metzler et al 1992) and CO (Brearley 1993) chondrites. In these objects, or more specifically in unbroken fragments within them, the texture consists of similarly-sized, dust-rimmed particles packed next to each other as if gently brought together and compressed, with no evidence for local fracturing or grinding.

Even after collisional effects associated with subsequent stages of growth have blurred this signal, perhaps even mixing material from different parent bodies, evidence remains in the bulk properties of all chondrite classes. Chondrite classes are defined by their distinctive mineral, chemical, and isotopic properties (*eg.* Grossman et al 1988, Scott and Krot 2005, Weisberg et al 2006). Large samples of material with a quite well defined nature were accumulated at one place and/or time, and material of a quite different, but equally well-defined, nature was accumulated at another place and/or time into a different parent body. Amongst the most obvious aspects of these class properties is a dominance within chondrites of sub-mm size mineral particles (generically "chondrules"; Grossman 1988, Jones et al 2000, 2005; Connolly et al 2006) which are aerodynamically well-sorted. Aerodynamic sorting of chondrite components was first emphasized by Dodd (1976), Hughes (1978, 1980), and Skinner and Leenhouts (1993), and has since been discussed by a variety of authors (see Cuzzi and Weidenschilling 2006 for a summary of the observations and arguments supporting aerodynamics). Chondrules have a size which varies from class to class, but is distinctive and narrowly defined within a given class or chondrite.

The evidence suggests that chondrules do not comprise merely a thin surface layer swept up by a large object (Scott 2006). In the case which we suggest as an archetype, the H-type ordinary chondrite parent body is widely believed to be a 100 km radius object (perhaps the asteroid Hebe), initially composed entirely of a physically, chemically, and isotopically homogeneous mix of chondrules and associated material, which was thermally metamorphosed by accreted ^{26}Al to a degree which varied with depth, into an onion-shell structure, and subsequently broken up in several stages (Taylor et al 1987, Tieloff et al 2003, McSween et al 2002, Grimm et al 2005). Bottke et al (2005) conclude from models of collisional evolution in the primordial (massive) and the current (depleted) asteroid belt, that the primordial asteroid mass distribution was dominated by objects having diameter of around 100km, rather than having a power-law size distribution somewhat like that of the current population.

We see the essential challenge as understanding how such a large object can be assembled from such a homogeneous mixture of mm-size constituents, while other objects (arguably the parents of the L and LL type ordinary chondrites as well, and logically then the parents of the chondrites of all classes) are assembled from distinct, yet comparably homogeneous, ensembles of qualitatively similar particles. Moreover this assembly, or primary accretion, phase of nebula evolution must persist for a duration of 1Myr or more between the formation times of the oldest and youngest meteorites (Wadhwa et al 2007) and even of objects found in the same meteorite. The > 1 Myr age spread between ancient refractory inclusions (CAIs) and chondrules is well known (Russell et al 2006), but there may even be a comparably extended age spread between different chondrules in a given meteorite (Kita et al 2005).

In recent years, radiometric dating of achondrites (melted meteorites) has revealed some early-formed (and early melted) planetesimals (Kleine et al 2005, 2006).

One expects early formation and melting to go together, because objects larger than only 10km or so, which accreted at the same time that refractory inclusions formed (4.567 Byr ago), would have incorporated their full complement of ^{26}Al and would have melted (LaTourette and Wasserburg 1998; Woolum and Cassen 1999, Hevey and Sanders 2006). Thus, early accretion implies melting, and lack of melting requires late accretion. Model results imply that, to avoid complete melting, 100km bodies must accrete only after a typically 1.5-2 Myr delay relative to ancient CAI minerals (reviewed by McSween et al 2002 and Ghosh et al 2006). While unknown selection and sampling effects may influence the limited meteorite data record, spectral analysis of the entire asteroid database also suggests that melted asteroids are rare. That is, while debate continues as to whether small amounts of melt might be found on the surfaces of many asteroids, which might be caused by impacts (*e.g.* Gaffey et al 1993, 2002), only Vesta and a handful of other examples of fully melted basaltic objects have been found in spite of extensive searches (Binzel et al 2002; Moskovitz et al 2007).

Put together, this body of information suggests that primary accretion started early but continued for several million years - thus, it was inefficient, or at least sporadic. By comparison, midplane incremental accretion in a nonturbulent nebula accretes numerous Ceres size bodies and tens of thousands of 10-100km size objects in only 10^5 years (Weidenschilling 2000); thus, it is highly efficient.

Models suggest that the density, temperature, and composition of the nebula evolved significantly over several million years (Bell et al 1995, D'Alessio et al. 2005, Ciesla and Cuzzi 2006). Thus one expects the properties of forming planetesimals to change with *time* even though the chemical, isotopic, and mineralogical properties of the mixture of solids from which they formed might have been fairly uniform in *space* at any *given* time (see Cuzzi et al 2003 and Ciesla 2007 for more detailed discussions). Reality might have been even more complicated - there is some evidence that chondrites of very distinct chemical and isotopic properties might have formed at roughly the same time (Kita et al 2005), suggesting a combination of spatial *and* temporal gradients.

In this paper we present the overview of a scenario by which accumulation of a well-defined particle mix into a large planetesimal - making it a "snapshot" of the local nebula mix - might occur sporadically or inefficiently in weak turbulence, over an extended period of time and throughout the terrestrial planet region. The challenge for the future is to show that the accretion processes discussed here can *quantitatively* account for the mass needed to build planetesimals of the mass needed to create planetary embryos and planets during the age of the nebula (Chambers 2004, 2006; Cuzzi et al 2007).

2.2. Turbulence

A variety of astronomical and meteoritical evidence supports weak, but widespread and sustained, nebula turbulence. The observed abundance of small particles at high altitudes above the midplane in many visible protoplanetary nebulae for millions of years is most easily explained by ongoing turbulence - both to regenerate the small grains in collisions and to redistribute them to

the observed altitudes (Dullemond and Dominik 2005). The survival of ancient, high-temperature mineral inclusions (CAIs) in chondrites, in spite of their tendency to drift inwards towards the sun, can also be explained by turbulent diffusion (Cuzzi et al 2003, 2005). Moreover, the recent discovery by STARDUST of both high- and moderate-temperature crystalline silicates in comet Wild2 (Brownlee et al 2007, Zolensky et al 2007) can be easily understood in this way (Ciesla 2007).

It remains a subject of active theoretical debate as to how, or even whether, the nebula can maintain itself in a turbulent state. Ongoing dissipation by molecular viscosity ν_m on the smallest, or Kolmogorov, lengthscale requires a production mechanism to continually generate turbulent kinetic energy. Although the very existence of ongoing disk accretion into the star, with the ensuing gravitational energy release, provides an ample energy source, the vehicle for transferring that energy into turbulent gas motions is undetermined. Baroclinic instabilities require substantial opacity at thermal wavelengths, but might be suitable to generate turbulence during the fairly opaque chondrule-CAI epoch in the inner solar system (Klahr and Bodenheimer 2003). The widely accepted magnetorotational instability (MRI) (Stone et al 2000) may or may not be precluded at the high gas densities of the inner solar system (Turner et al 2007). The role of pure hydrodynamics operating on radial shear remains unclear, because Keplerian disks are nominally stable to linear (small) perturbations (Balbus et al 1996, Stone et al 2000). However, a number of current theoretical studies suggest turbulence might indeed be present (*eg.* Arltdt and Urpin 2004, Busse 2004, Umurhan and Regev 2004, Dubrulle et al 2005, Afshordi et al 2005, Mukhopadhyay et al 2005, Mukhopadhyay et al 2006). Much of this recent work focusses on nonlinear (finite amplitude) instabilities occurring at the very high Reynolds numbers characterizing the nebula, which are well beyond the capability of current numerical and even laboratory models.

In this paper, we simply assume the presence of weak nebula turbulence. The intensity of turbulence may be characterized by a nondimensional parameter $\alpha = (v_t/c)^2$, where v_t is the velocity of the most energetic eddies and c is the sound speed. Values of α in the range $10^{-4\pm 1}$ are consistent with observed nebula lifetimes, and can be sustained by only a few percent of the gravitational energy released as the nebula disk flows into the sun. One then estimates the most energetic (largest) eddy size as $L \sim H\alpha^{1/2}$, where H is the nebula vertical scale height, or disk thickness. A cascade to smaller scales ensues, where the smallest (Kolmogorov) eddy scale is $\eta = L\text{Re}^{-3/4} \sim 1$ km and $\text{Re} = \alpha cH/\nu_m \sim 10^7$ for $\alpha \sim 10^{-4}$ is the nebula Reynolds number (Cuzzi et al 2001).

2.3. Turbulent concentration

It has been found both numerically and experimentally that particles of a well defined size and density are concentrated into very dense zones in realistic 3D turbulence (Eaton and Fessler 1994). The optimally concentrated particle has a gas drag stopping time t_s which is equal to the overturn time of the Kolmogorov scale eddies. In the nebula, $t_s = r\rho_s/c\rho_g$ where r and

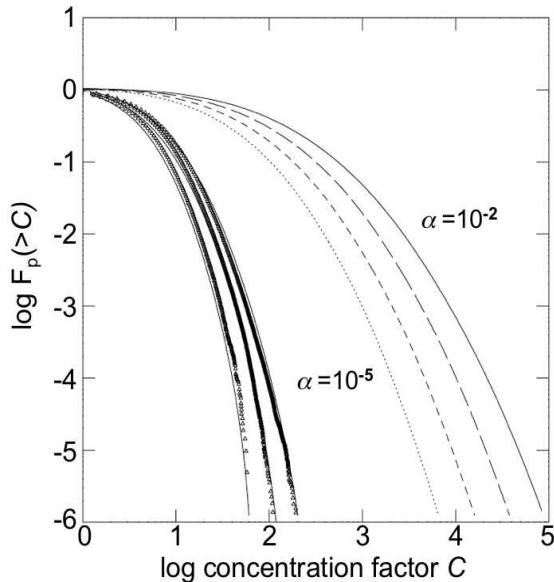


FIG. 1.— Cumulative probability distribution, or volume fraction F_p , of particles having local concentration factor larger than some value of C (from Cuzzi et al 2001; see also section 2.3). The curves with symbols represent comparison of the predictive theory described in Cuzzi et al (2001) with 3D numerical simulations at moderate Reynolds numbers; the curves without symbols are extension of the same theory to nebula conditions denoted by their values of α . Concentration factors $C \sim 100$ of chondrule precursors (leading to $\Phi = \rho_p/\rho_g \sim 1$) are fairly common for a range of nebula turbulent intensities (denoted by α), and help explain lack of chondrule isotopic fractionation (Cuzzi and Alexander 2006). In this paper we focus on the much less common, but much denser, regions towards the bottom right side of the plot ($C \sim 10^4$ or $\Phi \sim 100$). More general PDFs which separate out the role of vorticity and incorporate the effect of particle mass loading are discussed in section 2.3 and Appendix A.

ρ_s are the particle radius and material density, and c and ρ_g are the gas sound speed and density. The Kolmogorov eddy frequency ω_η scales with the orbital frequency Ω as $\omega_\eta = \Omega \text{Re}^{-1/2}$, and particles are most effectively concentrated when $t_s \omega_\eta \sim 1$ (Eaton and Fessler 1994). Chondrule-size silicate particles are concentrated for canonical nebula properties if $\alpha \sim 10^{-5} - 10^{-3}$; moreover the *shape* of the concentrated particle size distribution is parameter-independent, and agrees very well with that of chondrules (Paque and Cuzzi 1997, Cuzzi et al 2001). We define the concentration factor $C \equiv \rho_p/\bar{\rho}_p$, where we denote the local volume mass density of particles as ρ_p and $\bar{\rho}_p$ is its nebula average value, and the particle mass loading $\Phi \equiv \rho_p/\rho_g = C\bar{\rho}_p/\rho_g$. For instance, figure 1 (Cuzzi et al 2001) shows the probability distribution function (PDF) for C determined from numerical simulations at moderate Reynolds number (curves with symbols) and predicted for plausible nebula Reynolds numbers (curves without symbols). Note that the volume fraction having $C > 100$ is quite substantial, which helps explain some mineralogical and isotopic properties of chondrules (Cuzzi and Alexander 2006).⁵ Not surpris-

⁵ Here, $\Phi = \rho_p/\rho_g$ is different from the definition in Cuzzi and Alexander (2006), which is equivalent to $\rho_p/A\rho_g$, where $A \sim 10^{-2}$ is the fractional abundance of solids to hydrogen gas by mass. Thus values of Φ in Cuzzi and Alexander (2006) are the equivalent of $\rho_p/\rho_g \sim 1$ - a much more common occurrence than the situation we study here.

ingly, the volume fraction decreases for larger C . In this work we focus on the less abundant, but higher mass density, concentrations towards the lower-right hand side of the PDF.

The turbulent concentration PDFs of figure 1 did not allow for the feedback of the concentrated particles on the gas. This “mass loading” would be expected to damp gas turbulent motions once the particle mass density significantly exceeds that of the gas, and lead to a saturation of concentration at some value. Recent work which *includes* the feedback effects, through drag, of particle density on the damping of turbulence, has shown that values of $\Phi \leq 100$ can indeed be achieved - although less commonly than in the unloaded models such as shown in figure 1. This *cascade model* of turbulent concentration (Hogan and Cuzzi 2007) is summarized in Appendix A. Based on these results, we adopt $\Phi = 100$ as an upper bound in all stability and evolution modeling.

3. PRIMARY ACCRETION OF PLANETESIMALS

The ability of gravity to overwhelm opposing forces is a well-known theme in astrophysics, dating back 80 years to early studies of star formation by Jeans. Over 30 years ago, gravitational instability (GI) of solids in a dense layer near the nebula midplane was proposed to lead directly to solid planetesimals on a dynamical timescale (the orbit time) (Safronov 1969, Goldreich and Ward 1973). Traditional GI thresholds require the dynamical (collapse) time of a dense region $t_G = \pi(G\rho_p)^{-1/2}$, where G is the gravitational constant, to be shorter than both the transit time due to random velocity and the local shear (vorticity) timescale (Toomre 1964). These arguments imply that GI occurs when the local particle density exceeds a few times the Roche density $\rho_R = 3M_\odot/4\pi a^3$, where M_\odot is the solar mass and a is the distance from the sun (Safronov 1991, Cuzzi et al 2001). However, this scenario is frustrated by self-generated midplane turbulence even if the nebula is not globally turbulent (*e.g.* Weidenschilling 1980,1995; Cuzzi et al 1993,1994; Johansen et al 2007). That is, a dense layer of cm-size and larger particles orbits at a different velocity than the pressure-supported gas, leading to a vertical velocity shear which becomes turbulent and stirs the particle layer. A more recent flavor of GI requires the particles to be small enough that the particle-rich midplane acts as a single fluid, like fog, so that its vertical density stratification stabilizes it against self-generated turbulence (Sekiya 1998, Sekiya and Ishitsu 2001, Youdin and Shu 2002, Sekiya and Takeda 2003, Youdin and Chiang 2004). Because the particles must be very small to satisfy this *one-phase* requirement (mm-size and smaller), their settling towards the midplane is frustrated by even the faintest breath of nebula turbulence ($\alpha \sim 10^{-9}$). If the particles are prevented from settling into a sufficiently dense layer that their mass density can stratify the total density (eg, Dubrulle et al 1995, Cuzzi and Weidenschilling 2006), the conditions needed to trigger the instability are never achieved.

In the following subsections, we study the evolution of a dense clump such as might form towards the lower right domain of figure 1, albeit in a simplified way. We treat a clump as an isolated object when in reality it exists in a context of surrounding material of varying density. In section 4, we discuss the implications of more realistic

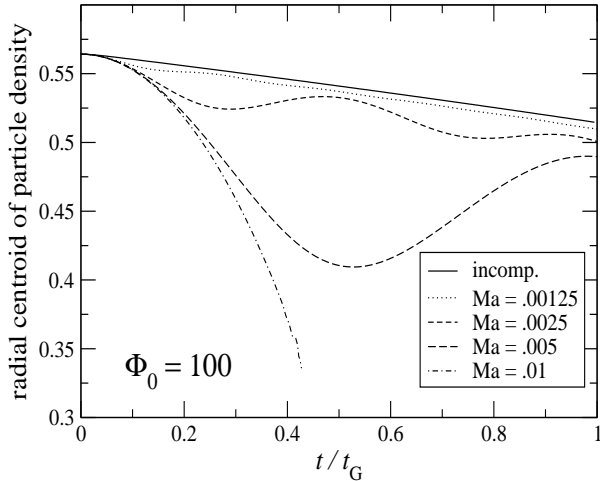


FIG. 2.— Results of a 1D compressible numerical model, showing how gas pressure precludes dynamical timescale gravitational instability (Sekiya 1983) as described in more detail in section 3.1. Here, $\text{Ma} = (l/c)(G\rho_g)^{1/2} = 1/\Phi^*$ is like a Mach number. Nebula values of c and ρ_g lie in the top set of nearly linear curves, allowing only slow inward sedimentation on the timescale t_{sed} (for $\Phi_0 = 100$). That is, under nebula conditions of gas density and temperature, and particle loading, the gas behaves as if it were incompressible and prevents dynamical timescale GI for particles with stopping time much less than the dynamical collapse time. conditions.

3.1. Gas pressure precludes particle gravitational instability

The role of the *gas pressure* in GI for nebula particles has been almost universally ignored, even though its importance was pointed out decades ago by Sekiya (1983). We encountered it ourselves independently. To test our GI thresholds, we initially ran numerical models of static, but very dense, clumps ($\Phi = 1000$), expecting them to collapse with gravitational free-fall or dynamical collapse times $t_G = \pi(G\rho_p)^{-1/2} = \pi(G\Phi\rho_g)^{-1/2}$ and velocities $V_G \approx l(G\rho_p)^{1/2}/2\pi$, where l is the clump diameter. We assumed a spherically symmetrical dense particle clump with density ρ_p , embedded in gas with density ρ_g , where $\Phi = \rho_p/\rho_g$. Instead, only very slow shrinkage ensued. We suspected that the collapse was being artificially blocked by our incompressible code.

We then developed a fully compressible 1D model which confirmed our incompressible calculations and clearly demonstrated a much higher, gas-pressure-dependent Φ threshold for GI in the limit when $t_s \ll t_G$. Results from the model are shown in figure 2.

Figure 2 shows results from this fully compressible model, illustrating how $\Phi > c/(l(G\rho_g)^{1/2})$ is required for traditional (dynamical timescale) instability to occur. The initial condition was a Gaussian blob having density distribution $\rho_p(r) = \Phi_0\rho_g \exp(-r^2/l^2)$. Slow shrinkage of the particles through the gas is seen in the stable, “incompressible” regime where nebula parameters lie, well within the flat curves at the top of the plot with $\text{Ma} \sim 10^{-4}$ for $l \sim 10^4 \text{ km}$, $c \sim 10^5 \text{ cm/s}$, and $\rho_g \sim 10^{-9} \text{ g cm}^{-3}$. The high value of Ma required for true dynamical timescale collapse (given the chosen value of $\Phi = 100$) would require smaller gas sound speed or larger clump size l and gas density ρ_g , by orders of magnitude.

The slow shrinkage in the stable regime results from particles sedimenting inwards towards their mutual center under their own self-gravity at their terminal velocity $v_T = gt_s$, where $g = 2G\Phi l\rho_g$ is the local gravitational acceleration due to the clump’s mass, and $t_s = r\rho_s/c\rho_g$ is the particle stopping time. Thus $v_T = 2G\Phi l r\rho_s/c \ll V_G$ for $t_s \ll t_G$, and the “sedimentation” timescale is

$$t_{sed} = \frac{l}{2v_T} = \frac{1}{4G\Phi(r\rho_s/c)} = \frac{c}{4G\Phi r\rho_s} = \frac{1}{4G\Phi\rho_g t_s}, \quad (1)$$

roughly 30-300 orbit periods at 2.5 AU for 300 μ radius chondrules and $\Phi = 1000-100$; that is, much longer than t_G . It seems inappropriate to describe this slow ongoing evolution as an instability - certainly in midplane scenarios where it was slow vertical sedimentation by individual particles toward the midplane that produced the “unstable” situation in the first place, and where only further slow sedimentation transpires. The situation is more akin to star formation mediated by ambipolar diffusion than by traditional gravitational instability. Gas pressure even precludes the Safronov-Goldreich-Ward GI in the form it was originally proposed, where cm-sized particles were envisioned (although t_{sed} would be faster for literally cm-sized particles, and more closely approaches t_G).

The results of Sekiya (1983) have apparently been overlooked by all subsequent workers, who have invariably assumed a Toomre-Safronov-Goldreich-Ward type *particle* ensemble which is decoupled from the gas, and stabilized (on small scales) only by particle random velocities. This gas pressure constraint is, however, crucial for particles in the chondrule size regime where $t_s \sim$ an hour and $t_G \sim$ a year, and must be applied to all GI models involving chondrule-sized particles. The good news is that for the interesting range of nebula gas density and particle concentration values, the gas *does* actually behave as if it were incompressible (validating the use of an incompressible code in numerical models such as shown in section 3.4).

The physics is easily understood in the one-phase regime ($t_s \ll t_G$). The particles feel no direct pressure force, but are firmly trapped to the gas which does. The (inward) gravitational force is dominated by particles for $\Phi \gg 1$. The particles drag and compress the gas with them as they begin to collapse under their self-gravity, producing a radial gas density gradient $d\rho_g/dl$; this translates into a large outward *pressure* gradient $c^2 d\rho_g/dl$ which acts on the gas, and thereby also on the strongly coupled particles.

The gravitational force per unit volume is $f_G = 4GM\rho_p/l^2 \sim 2G\Phi^2\rho_g^2 l$, where M is the clump mass and R its radius. After some incipient shrinkage and compression occurs, the outward pressure gradient force per unit volume becomes roughly $f_P = c^2 d\rho_g/dl \sim c^2\rho_g/l$, where c is the gas sound speed. Then for GI to be possible, $f_G/f_P = G\Phi^2 l^2\rho_g/c^2 > 1$, giving the criterion for GI as $\Phi > \Phi^*$, where $\Phi^* = c/(l(G\rho_g)^{1/2})$. Φ^* is like an inverse Mach number Ma^{-1} , where $\text{Ma} = (l/c)(G\rho_g)^{1/2}$. An alternate (perturbation) approach compares the incremental changes δf_P and δf_G associated with a small gravitationally induced shrinkage characterized by $\delta l \ll l$. It is straightforward to show (for $t_s \ll t_G$) that $\delta f_P/\delta f_G \approx$

$c^2\rho_g/GM\Phi \sim 10^5$ under nebula conditions. Thus the clump is “stiffened” by pressure and even a small incremental shrinkage is self-limiting. Inspection of **figure 2** shows small oscillations which suggest that a formal linear stability analysis might lead to an improved stability criterion; this is, however, beyond the scope of the present paper.

For $l \sim$ a few 10^3 km and $\rho_g \sim 10^{-9}$ g cm $^{-3}$ (De-sch et al 2005), $\Phi^* \sim 10^4$. This criterion for GI can be compared with the traditional criterion for (marginal, or maximal) instability which is widely used as *the* criterion for gravitational instability, roughly twice the Roche density $\rho_R = 3M_\odot/4\pi a^3$ (Goldreich and Ward 1973, Safronov 1991, Cuzzi et al 1993). The ratio of the two thresholds is:

$$\frac{\Phi^* \rho_g}{2\rho_R} = \frac{\rho_g}{2\rho_R \text{Ma}} \approx \frac{2c(G\rho_g)^{1/2}}{\Omega^2 l} \sim \frac{2 - 6 \times 10^3}{(l/10^3 \text{km})},$$

for $\rho_g = 10^{-10}$ to 10^{-9} . For the midplane GIs which have been widely discussed in the past (reviewed by Cuzzi and Weidenschilling 2006), $l \sim 10^2$ km, so the traditional GI criterion falls short by a factor of more than 10^4 (*cf.* Sekiya 1983)! This degree of mass concentration is unlikely under any plausible circumstances, especially for particles which are already well trapped to the gas. For the ubiquitous dense clumps we discuss here, which form at all elevations, $l \sim 10^4$ km. Thus the pressure-supported gas phase prevents the tightly coupled particles from undergoing GI until the particle mass loading is hundreds of times larger than the traditional GI criterion (which is on the order of the Roche density ρ_R).

Nevertheless, Sekiya (1983) also noted that when ρ_p is in the range usually cited for GI (a few times ρ_R , or $\Phi \sim$ a few hundred), a 3D “incompressible mode” arises which, while not explicitly stated, we interpret as retaining an identifiable cohort of particles. An “incompressible mode” might resemble a blob of water oscillating in zero-gravity. Dense zones which result from turbulent concentration are candidates for such incompressible modes, even at mass loadings too low to induce actual GI. However, the fate of such slowly evolving entities in the presence of likely perturbations has never been explored. Below we discuss the least avoidable, most pervasive disruptive perturbation which such clumps would encounter once they form, which we believe to be ram pressure disruption due to systematic velocity differences between the dense zones and the gas, and then derive conditions under which these clumps can survive to become planetesimals.

3.2. The fate of “incompressible” clumps

Several kinds of perturbation by the enveloping nebula gas might disrupt a dense clump before the slow sedimentation of its constituent particles towards their mutual center (on the timescale t_{sed}) can produce a moderately compact object.

Perhaps the simplest to discuss and dismiss are turbulent pressure, velocity, and/or vorticity *fluctuations* encountered by the clump. Turbulent pressure fluctuations on the scale l have typical intensity $\rho_g v_t(l)^2$, where $v_t(l)$ is certainly smaller than the fluctuating velocity $v_t(L) = c\alpha^{1/2}$ of the largest eddy (the dominant energy-containing eddy). The ratio of even the largest eddy

pressure fluctuations to the steady ram pressure from the headwind $\beta\Omega a = \beta v_K$ (a is the semimajor axis) is $(v_t/\beta v_K)^2 = \alpha c^2/\beta^2 v_K^2$. Since $c/v_K = H/a$ and $\beta = (H/a)^2$, $(v_t/\beta v_K)^2 < \alpha/\beta < 1$ unless $\alpha > 10^{-3}$. Nebula evolutionary timescales, and parameters leading to turbulent concentration of chondrule-sized particles in the asteroid belt region, imply $10^{-6} < \alpha < 10^{-3}$ depending on gas density and other properties (Cuzzi et al 2001). This suggests that turbulent velocity fluctuations on clump lengthscales play a small role. We have run simulations of clumps settling in gravity with and without enveloping turbulence, and the typical evolutions are qualitatively similar.

We next address local *average* vorticities on the length-scale of a clump. It has long been known that local vorticity is a factor in gravitational instability (Toomre 1964, Goldreich and Ward 1973). Because eddies much smaller than the largest scale of turbulence typically have larger vorticity than the Keplerian shear commonly explored (*eg.* Toomre 1964), this is a concern in principle. For example, in the inertial range, $\omega(l) \sim \Omega(L/l)^{2/3}$ (Tennekes and Lumley 1972). Then for $l \sim 10^4$ km, $L \sim H\alpha^{1/2}$ and $\alpha \sim 10^{-4}$, $\omega(l) \sim 10^4\Omega$. However, turbulent concentration has the property that dense particle zones preferentially lie in zones of locally *low* vorticity compared to the average at their lengthscale (Eaton and Fessler 1994). Statistical studies (Hogan and Cuzzi 2007) show that dense zones in high Re environments can form in regions with local vorticity 1-2 orders of magnitude smaller than the average value expected for that length-scale (see also figure 5). Below we sketch how such a constraint is derived and applied.

A simplified requirement for gravitational binding of a clump of lengthscale l and mass density ρ_p , in the presence of local rotation at angular velocity $\omega(l)$, is $4G\rho_p > \omega^2(l)$. Recalling that the local vorticity $\omega(l)$ can vary by orders of magnitude from its average value $\langle\omega(l)\rangle$, we normalize both sides of the above relationship between ρ_p and ω by the average inertial range enstrophy $\langle\omega^2(l)\rangle$, and define the normalized enstrophy $S = (\omega^2(l)/\langle\omega^2(l)\rangle)$. This quantity provides the horizontal axis on figure 5. Then the simple expression above can be rewritten as $\Phi > \langle\omega^2(l)\rangle S/4G\rho_g$. Inertial range relationships can be used to express $\langle\omega^2(l)\rangle = \Omega^2(L/l)^{4/3} = \Omega^2(L/B\eta)^{4/3}$ where η is the Kolmogorov scale and B is some scaling factor. Making use of $\text{Re} = \alpha cH/\nu_m = (L/\eta)^{4/3}$ as discussed earlier, and substituting nebula parameters at 2.5 AU, we find that gravitational binding requires $\Phi > 3 \times 10^6 \alpha S$. This constraint yields diagonal lines on plots of the sort shown in figure 5 (for an example see Cuzzi et al 2007). Interesting regions of parameter space remain accessible to a degree that depends on quantitative modeling of the PDF $P(\Phi, S)$.

Obviously, more detailed numerical models of clumps in realistic turbulence are needed to assess these perturbations. We will assume, for the purposes of this study, that turbulent pressure (and associated vorticity) fluctuations are a minor influence and that regions which are stable to their own local vorticity exist (see Cuzzi et al 2007). This leaves the dominant disruptive process, unavoidably shared by turbulent and laminar nebulae, as ram pressure disruption due to *systematic* velocity dif-

ferences between the clump and the gas, as described below. Incidentally, survival against ram pressure gives the horizontal stability boundaries in figure 3 of Cuzzi et al (2007). Emplacing these constraints on PDFs obtained from cascade models is somewhat involved, and a full quantitative description of the situation is deferred to a future paper.

3.3. Ram pressure disruption and the Weber number

Here, for simplicity, we envision the evolution of a single, isolated dense clump with $\Phi \gg 1$, merely as an example of one of the many dense clumps formed near the lower right hand corner of figure 1. The clump exerts a strong collective influence on the entrained gas, and the mixture experiences solar gravity as a unit. It attempts to move as an individual large object relative to the nebula gas, dragging the entrained gas along. For instance, a clump forming at some distance above the nebula midplane settles downward under the acceleration of the vertical component of solar gravity, whereas the surrounding gas remains under vertical hydrostatic balance. Also, nebula gas generally orbits at a slower velocity than the Keplerian orbit velocity v_K obeyed by massive particles. This is because of its generally outward radial pressure gradient force $-(1/\rho_g)dP/da = 2\beta\Omega a^2$, where a is the distance from the sun, and $\beta \sim 10^{-3}$. Thus, particles experience a headwind with magnitude $w_g \sim \beta\Omega a = \beta v_K \sim$ a few 10^3 cm/sec. These headwinds result in a ram pressure $\rho_g w_g^2/2$ which can disrupt a strengthless clump.

For example, a dense drop of ink settling in a glass of water is quickly disrupted by the Rayleigh-Taylor instability and mixes with its surroundings (Thomson and Newhall 1885). However, a dense drop of fluid *with surface tension* can avoid disruption and settle indefinitely at terminal velocity (as do raindrops, or water in oil). In this situation, the criterion for stability of a fluid droplet, which determines its terminal velocity and thence its size, is given by the Weber number We , where $We = 2r\rho_g v^2/\gamma$, and γ is the surface tension coefficient. Drops are disrupted when We exceeds some critical value $We^* \sim 1 - 10$ (Pruppacher and Klett 1997).

Dense particle clumps in the nebula have no surface tension, but they do have self-gravity. By direct analogy with the droplet surface tension criterion, we define a *gravitational Weber number* We_G as the ratio of the ram pressure force per unit area to the self-gravitational force per unit area for a flattened disk, which is the initial stage of a strengthless spherical clump of diameter l and particle density $\rho_p = \Phi\rho_g$ upon encountering a headwind w_g (Thomson and Newhall 1885). For a disk of surface mass density $\sigma_p = \rho_p l$, the gravitational force per unit area is $G\sigma_p^2$. Then

$$We_G = \frac{C_D \rho_g w_g^2}{2G\sigma_p^2} = \frac{C_D w_g^2}{2G\Phi^2 \rho_g l^2}, \quad (2)$$

where C_D is an effective drag coefficient for the clump, on the order of unity (see Appendix B). We_G can be written in other ways as well. The orbit frequency at a provides the useful relationship $\Omega(a) = (GM_\odot/a^3)^{1/2} \equiv (G\rho^*)^{1/2}$, or $G = \Omega^2/\rho^*$, where $\rho^* = M_\odot/a^3 \sim 3.8 \times$

10^{-8} g cm $^{-3}$ at 2.5 AU 6 ; then

$$We_G = \frac{C_D \rho^* w_g^2}{2\Phi^2 \rho_g \Omega^2 l^2} = \frac{C_D \beta^2 \rho^* a^2}{2\Phi^2 \rho_g l^2}. \quad (3)$$

By analogy with the more familiar surface tension case, there will be some critical *gravitational* Weber number for stability We_G^* , that is probably on the order of unity (Pruppacher and Klett 1997); its value must be constrained by numerical experiments as described below. Then we require for stability against headwind disruption that $We_G < We_G^*$ or

$$\Phi l > w_g / (2GWe_G^* \rho_g)^{1/2} = \frac{\beta a \Omega}{(2G\rho_g We_G^* / C_D)^{1/2}}. \quad (4)$$

These expressions determine the combination of clump diameter l and particle loading Φ that will stabilize it against a headwind of magnitude βv_K . The headwind due to nebula radial pressure gradient will occur even if a clump is at the midplane and has zero settling velocity; this gives the lower limit on ram pressure that the clump must be stable against. Neglecting vertical settling restricts potentially stable clumps to lying within about 0.01 gas scale heights of the midplane, where the headwind $\beta\Omega a$ is comparable to the vertical settling velocity. This restriction must be factored into statistical estimates of planetesimal production (see, e.g. Cuzzi et al 2007).

For typical nebula parameters, we assume gas density to be in the range $\rho_g = 10^{-10}$ g cm $^{-3}$ (a nominal minimum mass value) to 10^{-9} g cm $^{-3}$ (a more recent value supported by nebula evolution and chondrule formation; cf. Desch et al 2005), semimajor axis $a = 3.8 \times 10^{13}$ cm (2.5 AU), pressure gradient/headwind parameter $\beta \sim 10^{-3}$ (see, eg., Nakagawa et al 1986, Cuzzi et al 1993), and solar mass $M_\odot = 2 \times 10^{33}$ g. In this regime, $\Phi l > 1.5 - 5 \times 10^6 (\beta/10^{-3})$ km. Recall from section 2.3 and Appendix A that mass loading limits the maximum achievable mass loading to $\Phi \sim 100$. A clump satisfying the above constraint, with $l = 1 - 5 \times 10^4$ km, would have the mass of a 10-100 km radius body of unit density - thus, these precursors can lead to quite sizeable objects. This characteristic size range is intriguingly close to the roughly 50 km radius primordial building block size of Bottke et al (2005). The very existence of *any* preferred size for the primordial population, if true, is an intriguing result.

3.4. Numerical model of clump evolution

To obtain a sanity check on the concepts of section 3.3, and to constrain the (unknown) value of We_G^* for this problem, we developed a very simplified numerical model of a clump experiencing a steady nebula headwind from a more slowly orbiting, pressure-supported gas, using Hill's approximation which transforms a cylindrical system into a cartesian system rotating at some mean rate Ω_0 - useful if the domain covers a sufficiently narrow radial and angular region that the curvature is negligible. The overall orbital motion of particles (the Keplerian velocity) is thus subtracted out, and the gas exhibits a

⁶ Note ρ^* is different from Safronov's (1991) Roche density $\rho_R = 3M_\odot/4\pi a^3$ discussed earlier

small differential velocity because of its deviation from Keplerian. A particle clump under influence of the gas will slowly lag behind in the y (orbital) direction, and slowly drift to smaller x (radial) values, due to the gas headwind. The model is not intended to be a high-fidelity representation of a realistic nebula situation, but merely to check the basic Weber number model of section 3.3.

The code evolves the velocity field of a two-phase system. The gas is perturbed by a clump of particles, which are mutually attracted by gravitational forces and are themselves dragged by, and exchange momentum with, the gas. The Hill frame, with cartesian coordinates (x, y, z) , represents a radially narrow region corresponding to some range of radius a , orbital angle θ , and vertical distance Z , respectively. Periodic boundary conditions are used in all three dimensions. The instantaneous Navier-Stokes (Eulerian) equations describing the conservation of mass and momentum for the incompressible gas are expressed in the Hill frame as,

$$\nabla \cdot \mathbf{U} = 0, \quad (5)$$

and

$$\frac{\partial \mathbf{U}}{\partial t} + (\mathbf{U} \cdot \nabla) \mathbf{U} = \frac{\nabla P + \nabla P^{glob}}{\rho_g} + \nu \nabla^2 \mathbf{U} - 2\boldsymbol{\Omega}_0 \times \mathbf{U} + \mathbf{f}^{drag} + \mathbf{f}^{sp} \quad (6)$$

where \mathbf{U} is fluid velocity, ρ_g is gas mass density, ν is gas viscosity, P is local pressure (which fluctuates along with gas velocity and vorticity variations), $\nabla P^{glob} = (2\rho_g w_g \Omega_0, 0, 0)$ represents the (constant) global nebula radial pressure gradient, and $\boldsymbol{\Omega}_0 = (0, 0, \Omega_0)$ is the Kepler frequency vector. This setup causes the gas to flow towards the clump in the y direction at a uniform speed w_g . We are currently neglecting the Keplerian radial shear term $2q\Omega^2 x \mathbf{e}_x$, where $\Omega(a) = \Omega_0(a/a_0)^{-q}$ and $\Omega_0 = \Omega(a_0)$, in the gas and particle equations to get a better comparison with our analytical stability model. The shear rate associated with this term $(dw/dx)_{Kep} = \Omega_0/2$, whereas a typical (fluctuating) local shear or strain due only to turbulent motions is $(dw/dx)_{turb} \sim \omega(t) > \Omega_0$. Because the turbulent shear is so widely varying, and likely to be larger than the Keplerian shear, in this study we neglect both of these complications, though they are both suitable avenues for future work.

In our code, particles are followed in the Lagrangian sense. The term \mathbf{f}^{drag} represents the force per unit mass imparted to the gas by the particles. It has the general form

$$\mathbf{f}^{drag} = \frac{\rho_p}{\rho_g t_s} (\mathbf{V} - \mathbf{U}) \quad (7)$$

where \mathbf{V} is the mean weighted particle velocity at a grid point, t_s is the particle gas drag stopping time, and ρ_p is the particle mass density. To obtain \mathbf{V} , a weighted sum is carried out over particles in the eight cell volumes adjacent to each fluid grid point. Weighting functions are used which vary inversely with the distance of the particle from the grid point (Squires 1990, his section 5.1). Because of the periodic boundary conditions, the wake of a clump can impinge artificially on the clump from the upwind direction. To avoid this, we include the

term \mathbf{f}^{sp} in equation (6) as a ‘‘sponge force’’ per unit mass to restore the gas velocities downstream of the clump at the outflow boundary plane to their initial values \mathbf{U}_0 ; this ensures constant inflow values at the upstream boundary plane.

The sponge force has the form

$$\mathbf{f}^{sp} = \frac{1}{\tau_{sp}} (\mathbf{U} - \mathbf{U}_0), \quad (8)$$

where τ_{sp} is some time scale. The function $1/\tau_{sp}$ is modeled as a sigmoid in the y direction very near the outflow boundary. The parameters of the sponge were determined through test runs with the goals of minimizing the sponge’s spatial extent and maximizing its effectiveness without introducing numerical instabilities. Once determined, the same values were used for all production runs.

The (Lagrangian) equation describing the motion of particle i subject to the forces of gas drag and mutual gravity is (again neglecting the Keplerian shear term)

$$\frac{d\mathbf{V}_i}{dt} = 2\boldsymbol{\Omega}_0 \times \mathbf{V}_i + \mathbf{f}_i^{drag} + \mathbf{f}_i^{grav} \quad (9)$$

The term \mathbf{f}_i^{drag} describing the drag force per unit mass on particle i by the gas takes the form

$$\mathbf{f}_i^{drag} = \frac{1}{t_s} (\mathbf{U}(\mathbf{X}_i(t)) - \mathbf{V}_i(t)), \quad (10)$$

where $\mathbf{U}(\mathbf{X}_i(t))$ is the gas velocity interpolated to the particle’s position $\mathbf{X}_i(t)$ at time t .

Finally, the mutual gravity force per unit mass on each particle is

$$\mathbf{f}_i^{grav} = G \sum_{j \neq i}^{N_p} m_j \frac{\hat{\mathbf{X}}_{ij}(t)}{(|\mathbf{X}_{ij}(t)| + \epsilon)^2} \quad (11)$$

where G is the gravitational constant, and N_p is the number of particles. $\hat{\mathbf{X}}_{ij}$ is the unit vector associated with the distance $\mathbf{X}_{ij}(t) \equiv \mathbf{X}_i(t) - \mathbf{X}_j(t)$ between particles j and i , and ϵ is a constant that softens the force at small separations to prevent numerical singularities, chosen to be comparable to a grid cell in extent.

Eqs. (6) and (9) are solved using pseudo-spectral methods commonly used to solve Navier-Stokes equations for a turbulent fluid (Canuto et al 1987). Periodic boundary conditions are assumed and the number of nodes used in each direction is generally 128, 256, 128 with a spacing of $2\pi/64$. A Fast Fourier Transform (FFT) algorithm is used to evaluate the dynamical variables \mathbf{U} at the computational nodes. A second-order Runge-Kutta scheme is used to time-advance the gas and particle velocities. A third-order Taylor series interpolation scheme is used to determine gas velocities at the particle positions from values at the eight nearest neighbor nodes. The mutual gravity calculation is done in a brute force fashion with a N_p^2 algorithm to evaluate the force contributions from all particles. The code is written in Fortran 77 and is parallelized using OpenMP directives. The FFT calculations are done simultaneously on the planes perpendicular to the y and z axes, and all loops involving particle indices are parallelized. Typically, 3000 ‘‘superparticles’’

are used, but some runs used more than 20000. Each “superparticle” represents the dynamical effects, and typical response, of a large number of actual chondrules.

Initially the particles are arranged in a uniform spherical clump. The initial velocities for the gas and the particles inside and outside the clump are determined from the expressions in Nakagawa et al. (1986):

$$\begin{aligned} \mathbf{U}_0 &= w_g \frac{\rho_p}{\rho_g + \rho_p} \left(\frac{2D\Omega}{D^2 + \Omega^2}, \frac{D^2}{D^2 + \Omega^2} - \frac{\rho_g + \rho_p}{\rho_p}, 0 \right) \\ \mathbf{V}_0 &= -w_g \frac{\rho_g}{\rho_g + \rho_p} \left(\frac{2D\Omega}{D^2 + \Omega^2}, \frac{D^2}{D^2 + \Omega^2}, 0 \right) \end{aligned} \quad (13)$$

where $D = (\rho_g + \rho_p)/\rho_g t_s$. The initial velocity of the gas outside the clump is found by setting $\rho_p \rightarrow 0$ in equation (12): $\mathbf{U}_0 = (0, -w_g, 0)$; inside the clump the specific case value of Φ is used in equations (12) and (13) to initialize the gas and particle velocities.

Runs with single particles of different t_s were made to verify that the Nakagawa et al. (1986) initial conditions are steady state solutions for the particle equations. The wallclock time to evolve one integration step is 0.7 sec using 256 Intel Itanium 2 processors running at 1.5 gihertz. The wallclock time to evolve 1 orbital period is 121 hours.

3.5. Results of the numerical model

Figure 3 shows how, as predicted by the simple theory of section 3.3, certain combinations of clump mass loading Φ and dimension l remain stable against ram pressure disruption for nebula headwinds produced by a pressure gradient characterized by β . We is dimensionless, and the second expression in eqn. (2) can be used to obtain the critical value of We_G which separates stable from unstable configurations of the clump, $We_G = We_G^*$, directly from measured values in code units (see Appendix B). We expect that We_G^* will be in the range 1-10. The combination of parameters in the stable case shown (right panels) gives $We_G^* \sim 1$; if self gravity is turned off, the clump is disrupted in $t_{dis} \sim 1/2\pi$ orbits, whereas it will sediment into itself on a timescale $t_{sed} \sim 8$ times as long (see Appendix B). In the stable cases, a dense core is seen to continually shrink and become denser throughout the run, even as material is shed from the periphery of the clump, such that the value of Φl for the core continues to increase (see Appendix C, **figure 7**).

The numerical clump models exhibit considerable erosion over the duration of the runs from a viscously stirred surface layer, and this gradual but inexorable mass loss might lead to their disruption if arbitrarily long runs were practical at this time. However, as discussed in Appendices B and C, this large amount of erosion is a gross overestimate of what would happen in the nebula, because numerical viscosity (and consequently shear around the periphery of the clump) plays a far larger role in the current numerical models than it ever would in the actual nebula. That is, the viscously stirred and eroded surface layer in the numerical clumps contains orders of magnitude more mass than would be the case for a nebula clump of the size and density required to survive ram pressure disruption (see Appendix B). In Appendix C, we describe the movies from which **figure 3** is taken and also show how the protected inner regions of the clumps

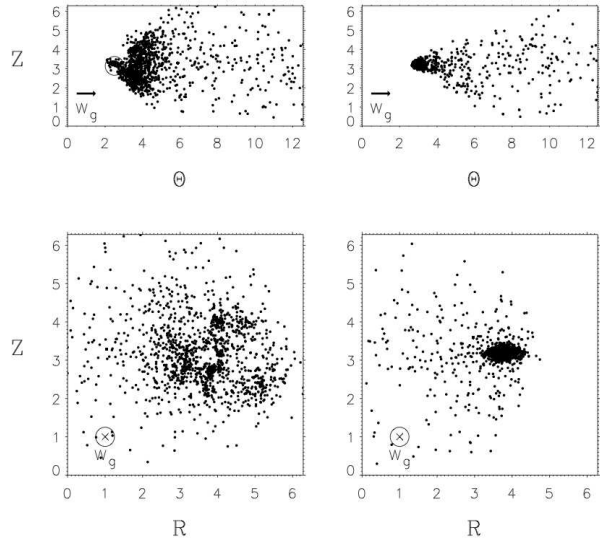


FIG. 3.— Snapshots from evolutionary models of dense clumps experiencing a nebula headwind without (left column) and with (right column) self-gravity. Top row: projected into a vertical plane ($z-\theta$); bottom row: projected onto the $a-z$ plane ($a-\theta$ projections are similar), with the gas inflow into the page. In the top left panel the open circle shows the initial size and position of the clump. After less than an orbit, ram pressure disrupts the gravity-free clump (left) but the gravitating clump is stable (right) and continuing to shrink inexorably, even while being eroded. Movies showing this evolution are available online (see Appendix C).

are behaving exactly as predicted, both in stable and unstable regimes. For more realistic, larger clump Re_c in the nebula, a far larger fraction of the clump mass will show this behavior rather than being artificially eroded.

The primary purpose of the numerical models is merely to provide an independent sanity check on the physics of our Weber number model and obtain some idea of We_G^* , which gives us an order-of-magnitude estimate for the product Φl which nebula clumps require to survive headwinds of a particular $\beta\rho_g$. Future coding improvements are needed to allow larger (higher Re_c) clumps which would more closely approach nebula conditions in terms of their balance between pressure forces and viscous forces (see Appendices B and C); these improvements will probably include an implicit time advance for the drag terms and perhaps also a tree or particle-in-mesh code for the particles.

4. DISCUSSION AND SUMMARY:

We have shown how self-gravity can stabilize dense clumps of mm-sized particles, which form naturally in 3D turbulence, against disruptive gas ram pressure on timescales which are sufficiently long for their constituent mineral grains to sediment towards their mutual centers and form physically cohesive “sandpiles” of order 10-100km in size. The essence of the result is a critical “gravitational Weber number” on the order of unity, in which self-gravity plays the role of surface tension in more familiar situations such as raindrops. Characteristic mass densities and lengthscales are determined which meet this requirement. We show numerical results which are in general agreement with the predictions of the simple theory, for isolated, spherical initial clumps.

The scenario we have sketched out leads from aerody-

namically size-sorted nebula particles, having the properties of chondrules, to sizeable planetesimals formed entirely from such particles which contain a snapshot or grab-sample of the local particle mixture. Turbulent concentration first produces the dense zones of size-sorted particles. The more common, less dense of these regions may provide typical chondrule melting environments (Cuzzi and Alexander 2006). Some of the less common, very dense zones, which we have shown elsewhere can achieve mass densities 100 times larger than that of the gas, have the potential to become planetesimals depending on their lengthscales, nebula location, and local vorticity. It is intriguing that our characteristic stabilized clump masses are not far from the mass inferred by Bottke et al (2005) to represent a typical primordial object in the pre-dispersal, pre-erosional asteroid belt.

Ultimately, the sandpiles resulting from completed sedimentation will become compacted further by inevitable collisions with other sandpiles, leading to today’s fairly dense asteroids, while retaining a physical and chemical memory of their parent particle clumps. The mechanism is easily extended to the unmelted aggregate particles of the outer solar system, where, however, if chondrules are absent, the size-sorting fingerprints of the process (Cuzzi et al 2001) might be less evident.

The conclusions of this paper differ from the suggestions in Cuzzi et al (2001), who focussed on the possible role of ultra-dense clumps with size comparable to a Kolmogorov scale (0.1 -1 km). Since that time, Hogan and Cuzzi (2007) found that particle mass loading saturates the value of $\Phi = \rho_p/\rho_g$ at a value of about 100, redirecting our attention to larger clumps in the $10^3 - 10^4$ km size range. Clumps and fluid structures of these large sizes are much more accessible with numerical codes, both of the standard direct simulation type and the cascade type (Appendix A).

In this scenario, primitive bodies may not primarily represent spatial, but perhaps temporal, samples of the particulate contents of the nebula as its chemical, physical, and isotopic properties evolve over several Myr. The temporal, as well as the spatial, variation in the physical, chemical and isotopic properties of the concentrated particles, which are being continually altered by thermal events and mineralogical alteration in the nebula gas, can then help account for class-to-class variations between the chondrite groups. An implication of this drawn-out, inefficient process is that younger chondrite types should contain evidence of “leftovers” or “refugees” from earlier times, which escaped primary accretion. Several aspects of chondrite makeup are compatible with this implication. Of course, it is well known that ancient CAI minerals and less-ancient, less refractory Amoeboid Olivine Aggregates are found alongside much younger objects in the same chondrites (*eg.* Scott and Krot 2005). Also, the oldest chondrites (CVs) contain primarily type I chondrules (which have an age observationally indistinguishable to that of CAIs) and no (more oxidized, heavier O-isotope) type II chondrules, while the younger ordinary chondrites contain a mixture of type I and type II chondrules, some with hints of age variation even within a given chondrite (Kita et al 2005). The oldest and first-formed objects are all likely to have melted from

their abundant ^{26}Al (Kleine et al 2005, 2006; Hevey and Sanders 2006), producing differentiated achondrites and metallic objects, so it is no longer possible to dissect their primordial components.

Of course, the real world is more complicated. Some complications are meteoritic: as only one example, CO chondrites and ordinary chondrites appear to be about the same age (younger than CV chondrites), but have very different chemical and isotopic properties (Kita et al 2005), which would, in the context of this scenario, argue for some degree of spatial (radial?) variation in the makeup of nebula particulates at that time anyway.

On the theoretical side, of course, self-consistent numerical models which follow clump evolution in realistic turbulence with headwinds and vertical settling need to be pursued, to check these preliminary assessments which make simplistic assumptions about the local headwind and assume isolated clumps. Several recent studies have found that transient “pressure ridges” arise in the gas in association with spiral density waves or vortical structures (Haghighipour and Boss 2003, Rice et al 2004, Johansen et al 2007); in such regions, the local radial pressure gradient and headwind diminish (other regions will have unusually *large* headwinds). Moreover, clumps do not exist in isolation, but more realistically as a dense core within a larger, less dense envelope which weakens the headwind felt by the dense clump core relative to the nebula average we characterize by β . Both of these conditions would allow some clumps to survive with smaller Φl . Other complications include interactions between different strengthless objects, leading to mergers or disruptions.

Our stability criteria are most likely to be satisfied in a region fairly close to the nebula midplane ($\sim 0.01H$, see section 3.3), because at higher altitudes the vertical component of solar gravity leads to vertical settling of dense clumps at higher terminal velocities than are easily stabilized against. However, this vertical settling, even if it leads quickly to disruption of individual clumps, enhances the downward transport rate of small particles and increases the solid/gas ratio closer to the midplane from that generally predicted by simple 1D diffusion models (*eg.*, Bosse et al 2006).

All these effects have implications for the occurrence frequency of clumps of the requisite Φl for stability. Quantitative statistical determinations of the volume fraction of stable clumps which can become planetesimals at any given time will use, for instance, approaches such as the cascade models described in Appendix A. Simplified, preliminary work exploring these factors indicates that, while the volume fraction of stable clumps is low at any given time (so the process is clearly not an efficient one), accretion rates are roughly an Earth mass per Myr in the asteroid belt region (Cuzzi et al 2007). However, considerable work remains to establish the statistical formation rate of appropriate clumps capable of following this evolutionary path and to study the evolution of clumps in realistic turbulence, with variable headwind velocity and simultaneous vertical settling.

We thank J. Eaton, M. Gaffey, P. Goldreich, W. Hartmann, G. Laughlin, K. Sreenivasan, K. Squires, and A. Wray for very helpful conversations on various aspects of

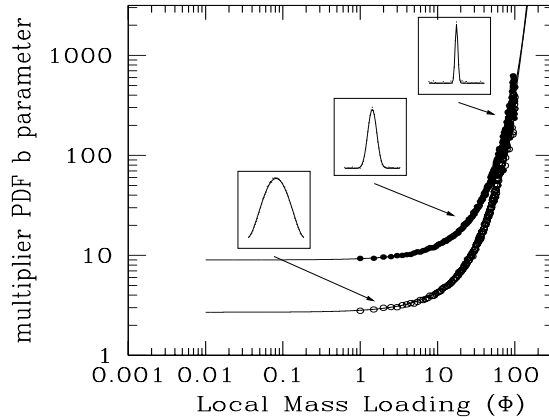


FIG. 4.— Conditioning curves for multipliers $p(m)$; the parameter b depends on the local mass loading Φ ; larger b indicates a narrower PDF $p(m)$. Open symbols: for particle concentration C ; filled symbols: for enstrophy ($S = \omega^2$). The small insets show $p(m)$ at several values of Φ . From Hogan and Cuzzi (2007).

this research, and A. Wray, A. Dobrovolskis, P. Garaud, and S. Weidenschilling for thorough reviews of the original manuscript and a number of useful comments which have been included. N. Turner and A. Carballido also provided useful comments on an earlier version. This work was supported by a grant to JNC from NASA’s

Planetary Geology and Geophysics program. Generous grants of cpu time from NASA’s HEC program were essential to the progress of this research; we thank E. Tu, K. Schulbach, C. Niggley and R. Pesta in particular for their help along these lines. We also thank J. Chang for coding optimization assistance.

APPENDIX

APPENDIX A: MASS LOADING AND THE CASCADE MODEL

This aspect of our work incorporates two related and important concepts: that of *intermittency*, and that of a statistical cascade process. For instance, it is widely known that dissipation of turbulent kinetic energy occurs at the Kolmogorov scale; it is less widely known that the spatial distribution of dissipation, like that of the particle concentration factor C , is highly *intermittent*. Intermittent quantities are spatially and temporally unpredictable, and fluctuate increasingly with increasing Reynolds number Re . However, the statistical properties of intermittent quantities like C (their probability distribution functions or PDFs) are well determined on any lengthscale. In what follows, it will be necessary to distinguish between two closely related quantities: the concentration C and the mass loading $\Phi = \rho_p/\rho_g = C\bar{\rho}_p/\rho_g$. This is because the emergence of particle feedback on the gas due to mass loading (Φ), depends both on C and on the initial value of $\bar{\rho}_p$. It is ultimately C that is evolved in the cascade, but *how* it evolves depends on Φ . So both quantities will be alluded to in parallel.

In its inertial range, which is extensive at high Re , turbulence is a scale-free process that is often referred to as a cascade and inspired the approach of cascade modeling (Meneveau and Sreenivasan 1991). The physics of transport of kinetic energy, vorticity, and dissipation from their sources at large scales is independent of scale until viscous processes enter at the smallest (Kolmogorov) scale. Scale-independence and Re -independence are connected because Re determines the depth of the inertial range: $Re^{3/4} = L/\eta$ (Tennekes and Lumley 1972). Cascade models simplify this complex, nonlinear, 3D scale-free process into a set of partition rules which are independent of scale, or of *level* in the cascade. Larger Re means a larger number of eddy spatial bifurcations (or levels) between L and η , and stronger fluctuations in intermittent properties (Meneveau and Sreenivasan 1991). Cascade models don’t preserve all the information of full 3D models (such as the tubelike spatial structures characterizing vorticity) but they do reproduce the statistical properties (the PDFs), which are of primary importance for our problem. The successful use of such models to describe the intermittency of dissipation, and other quantities, in turbulence (Juneja et al 1994, Sreenivasan and Stolovitsky 1995) led us to pursue a cascade model for turbulent concentration of particles.

A cascade model consists of a set of “multipliers” - fractions which define how a quantity of interest is unequally partitioned from a fluid parcel at some level, into its equal-sized subdivisions at the next level. The PDF of particle concentration factor C is determined over all the numerous end-level outcomes of applying a multiplier m (chosen from its own PDF $p(m)$) to each volume element as it bifurcates at each level of the cascade. It has been observed that $p(m)$ is independent of level in the turbulent inertial range (Sreenivasan and Stolovitsky 1995). Hence, multiplier PDFs determined from a direct numerical simulation (DNS) at low Re (with a relatively small number of levels), merely applied repeatedly over additional levels, can *predict* the properties at higher Re (if nothing changes in the physics). Our cascade model (Hogan and Cuzzi 2007) uses a common form for $p(m)$: $p(m) \propto m^{b-1}(1-m)^{b-1}$, where the parameter b determines the width of $p(m)$ (Sreenivasan and Stolovitsky 1995). Both the concentration C and the vorticity ω are described by their own b -distributions. Multiplier PDFs with small b ($b \leq 1$) are broad, and in them

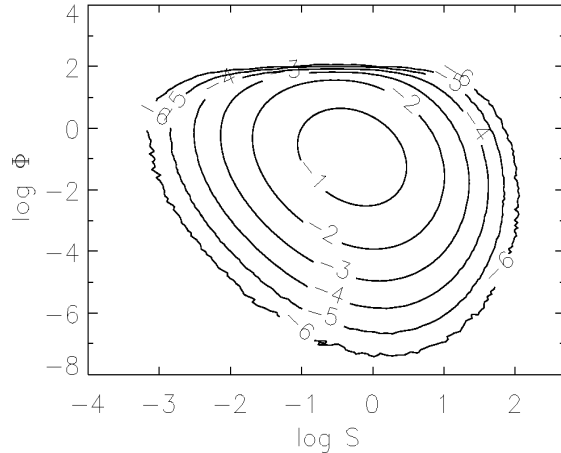


FIG. 5.— Joint (binned) probability $\Phi\omega^2 P(\Phi, \omega^2)$ from the conditioned cascade model, for a 24-level case with initial $\overline{\rho_p}/\rho_g = 10^{-2}$. The curves of figure 1 are the S -averaged equivalent of this plot (and show C instead of Φ), but do not include the effects of mass loading. Note the flattening or saturation at $\Phi \sim 100$, reflecting the near-vertical asymptote of the conditioned- b curve of figure 4 at $\Phi \sim 100$. A 24-level cascade is in the plausible range for clumps of size $\sim 10^4$ km in a nebula with $\alpha \sim 10^{-3} - 10^{-4}$. In this figure, the enstrophy S is normalized to its mean value for the binning lengthscale (from Hogan and Cuzzi 2007).

multipliers much different from $m = 0.5$ occur with higher probability, producing a grainier, more intermittent spatial distribution. PDFs with large $b (\gg 1)$ are narrow and centered on $m = 0.5$; because each “eddy bifurcation” then involves a nearly 50-50 partitioning, the resulting spatial distribution is nearly uniform and subsequent growth of Φ becomes more difficult.

The cascade model can then be used to address the issue of how particle mass loading can affect the cascade - that is, change the physics as the cascade progresses. This dependence is known as *conditioning* of a cascade. We found that the process can be represented quite well as two separate *one-phase* conditioned cascades for C and ω in which multiplier distributions $p(m)$ for both C and ω depend only on the local particle mass loading Φ . We used our full 3D numerical simulations to establish how b for both these properties depends on local particle or fluid properties.

Figure 4 shows conditioning curves for both C and ω (the latter expressed as enstrophy $S = \omega^2$), as extracted from multiple 3D DNS simulations at various Re as large as 2000 (Hogan and Cuzzi 2007). Note how the multiplier PDFs extracted from the DNS results (shown using insets) get narrower (have larger b) as mass loading increases, choking off intermittency. In these runs, $\overline{\rho_p}/\rho_g = 1$, so $C = \Phi$. These results establish the upper limit $\Phi \sim 100$ which can be obtained by turbulent concentration, regardless of the initial value of $\overline{\rho_p}/\rho_g$. In the nebula, with a smaller initial $\overline{\rho_p}/\rho_g$, higher Re or deeper cascades (and larger ensuing C values) are needed to reach this saturation point.

To determine the joint PDF of concentration C and vorticity ω , we require not only the conditioned multipliers for ω^2 and C (**Figure 4**), but also their spatial correlation. Hogan and Cuzzi (2007) found, on average, a 70-30 preference for anticorrelation at each partitioning, consistent with previous observations that particle concentration zones avoid zones of high fluid vorticity (Squires and Eaton 1990, 1991; Eaton and Fessler 1994; Ahmed and Elghobashi 2000, 2001). Including this partitioning asymmetry factor as a weighted coin gives us a two-phase (particle-gas), conditioned cascade model which shows very good agreement with the joint PDF $P(\Phi, \omega^2)$ directly determined from our full 3D mass loaded simulations (see Hogan and Cuzzi 2007). However, to match the full 3D DNS simulations at Re = 2000, the cascade model needs only about 15 levels, taking about 10 cpu-hours (for 1024 realizations) compared to over 90000 cpu hours to converge our full 3D simulation.

Using these conditioned multipliers and asymmetry factor, entire PDFs of particle concentration (mass loading) and vorticity can be generated for arbitrary numbers of levels (arbitrary Re). For example, the 24 level model of **Figure 5** (from Hogan and Cuzzi 2007) is of direct relevance for $10^3 - 10^4$ km scale dense zones of interest for the nebula. **Figure 5** illustrates the saturation of the particle concentration at $\Phi = 100$ and the fact that high Φ occurs preferentially at low enstrophy or vorticity. The upper left quadrant is of most interest for determining the *numbers* of clumps which can survive to become planetesimals (see Cuzzi et al 2007 for more details).

APPENDIX B: SCALING BETWEEN NUMERICAL CODE AND NEBULA

While the primary result of this paper - the existence of some stability regime determined by a critical gravitational Weber number We_G^* - can be expressed in a nondimensional way, some aspects of the results (specifically the numerical results and the inferred value of Φl for the nebula) require us to pursue the relationship between nebula parameters and code units more deeply. Values in code units are denoted by primes below. The fundamental quantities in the problem are (1) the gas and particle densities ρ_g and $\rho_p = \Phi\rho_g$; (2) the clump diameter l ; (3) the local orbit frequency $\Omega(a)$ where a is the distance from the sun; (4) the local radial pressure gradient $dP/da = dP/dx$, where x is in the Hill frame; (5) the particle stopping time t_s ; (6) the velocity of material in the Hill frame \mathbf{W} , that is, relative to Keplerian, where \mathbf{W} represents either the particle or gas velocity; and (7) the gravitational constant G . The principal forces are

the coriolis force due to the rotating frame $-2\Omega_0 \times \mathbf{W}$, the pressure force $(-1/\rho_g)dP/dx$, and the gas drag forces that couple the gas and particles (section 3.3). The code unit of length is radians (the domain is 2π radians on the short dimension (x or z) and the grid cell size is therefore $\Delta = 2\pi/N$ where N is the number of grid points along that axis). The code time unit (ctu) is $1/\Omega'$ where $\Omega' = 1$ is the code value of rotation frequency; thus the orbit period is 2π in code time units or ctu. We treat as equivalent $a = R = x$.

As noted in section 3.3,

$$\Omega(a) = (GM_\odot/a^3)^{1/2} \equiv (G\rho^*)^{1/2}, \quad \text{or} \quad G = \Omega^2/\rho^*$$

where $\rho^* = M_\odot/a^3 \sim 3.8 \times 10^{-8} \text{ g cm}^{-3}$ at 2.5 AU (note this is different from Safronov's (1991) Roche density $\rho_R = 3M_\odot/4\pi a^3$). To normalize mass and mass density (and ultimately establish the code value of the gravitational constant G') we assume a nebula gas mass density $\rho_o \sim 10^{-10} \text{ g cm}^{-3}$ (minimum mass nebula; Cuzzi et al 1993) at 2.5 AU; then code quantities $\rho'_g = \rho_g/\rho_o = 1$ and $\rho'_p = \rho_p/\rho_o = \Phi\rho'_g = \Phi$, and $\rho'^* = \rho^*/\rho_o$. Also, in code units $\Omega' = \Omega/\Omega_0 \equiv 1$ where $\Omega_o = \Omega(a_o)$ is the actual orbit frequency at the region of interest. Then the gravitational constant in code units, G' , can simply be written as $G' = \Omega'^2/\rho'^* = 1/\rho'^*$. Finally, the pressure force is written as

$$-\frac{1}{\rho_g} \frac{dP}{dx} \equiv 2\beta a \Omega^2 = 2\beta a G \rho^* = 2w_g \Omega,$$

where $\beta \approx 10^{-3}$ is typical (Nakagawa et al 1986; Cuzzi et al 1993), $G' = \rho_o/\rho^* = 3 \times 10^{-3}$. Then the dimensionless parameters Φ and l' are set to satisfy various constraints of the code (resolvable clump, adequate particle statistics, reasonable timescale, etc) and β' is allowed to vary, to determine empirically the critical value of We_G^* as the largest value of We_G that remains stable. That is, we want l' to be large enough such that the clump is well resolved, but not so large that it fills the entire cross section of the computational box. Typically l' is only 10-20 grid cells so far, and as noted below, this exaggerates the viscous stresses and surficial erosion of material. We want Φ to be large enough that the clump is much denser than the gas, and we want a large enough number of particles to act like a continuum. The value of t_s should ensure that the clump sedimentation time t_{sed} is larger than its ram pressure disruption time t_{dis} (see below), to provide a real test that self-gravity is preserving the clump rather than simple collapse.

Important timescales in the numerical model

The dynamical collapse time of the clump under its own self-gravity, and in the absence of gas pressure, is $t_G = \pi(G\rho_p)^{-1/2}$, or in code units $t'_G = \pi(G'\Phi)^{-1/2}$. The mass loading which produces a clump dynamical time comparable to the orbit time is then obtained using $\pi(G'\Phi)^{-1/2} = 2\pi/\Omega' = 2\pi$ or $\Phi = 1/4G' \sim 100$, again in fair agreement with prior expectations. However, gas drag prevents clump collapse on this timescale, as described in section 3.1, and actual shrinkage takes a time t_{sed} (eqn. 1). The number of orbits over which we need to follow the clump to ensure it really survives is roughly

$$\frac{t_{sed}\Omega}{2\pi} = \frac{c\Omega}{8\pi G\Phi r \rho_s} = \frac{H\Omega^2}{8\pi G\Phi r \rho_s} = \frac{\Omega^2}{G\rho_s} \frac{H}{r} \frac{1}{8\pi\Phi} = \frac{\rho^*}{\rho_s} \frac{H}{r} \frac{1}{8\pi\Phi},$$

where we have used $c = H\Omega$. This expression can be assessed using real quantities, and is 30-300 orbits for particle radius 300μ and mass loading $\Phi = 1000 - 100$. This behavior ($t_{sed} \gg 2\pi/\Omega'$) can be controlled in the code, once the other parameters are established as above, by adjusting the particle stopping time t_s . Because of long code run times, at present we are limited to stipulating only that the sedimentation time significantly exceeds the nominal (self-gravity-free) disruption time; that is, $t_{sed} \gg t_{dis}$, where

$$t_{dis} \approx (l/w)\sqrt{2\Phi/C_D}.$$

This expression for the disruption time t_{dis} is derived from the ram pressure force (sect 2.3) by setting the distance traveled in time t by the windward half of the clump, under acceleration by the ram pressure force, equal to the clump diameter (assuming the leeward half of the clump doesn't get accelerated), and solving for t . The value of C_D for our clumps is on the order of unity, as we verify below.

Numerical viscosity and the clump Reynolds number:

The code calls for some input viscosity ν' ; with it, the Reynolds number of the clump having diameter l' radians, in a headwind of speed w'_g (in code units of radians per ctu), is $Re'_c = l'w'/2\nu'$ where $\nu' = 0.1$ is the defined code viscosity (radians²/ctu). We assume an inertial range expression within the wake of the clump to determine the wake's Kolmogorov scale: $\eta'/l' = Re'_c{}^{-3/4}$, and thus $\eta' = (2\nu'l'^{1/3}/w'_g)^{3/4}$ radians. Our highest resolution runs to date had a gas relative velocity $w'_g = 38$ radians/ctu and used a clump size $l' = 2$ radians. The nominal Kolmogorov scale associated with this flow is $\eta' = (2(0.1)(2)^{1/3}/38)^{3/4} \sim 0.02$ radians (compared to the grid cell size of 0.05-0.1 radians); the wake turbulence is thus under-resolved and the code's true viscosity is numerical: $\nu'_n \sim w'_g \Delta$ (at the boundary of the clump).

While we are not concerned with the fine-scale details of the wake, this marginal resolution introduces some caveats. The ratio of ram pressure force to viscous force (both per unit area) is, in general, $(\rho_g w_g^2/2)/(\rho_g \nu dw_g/dr) \sim w_g l/4\nu =$

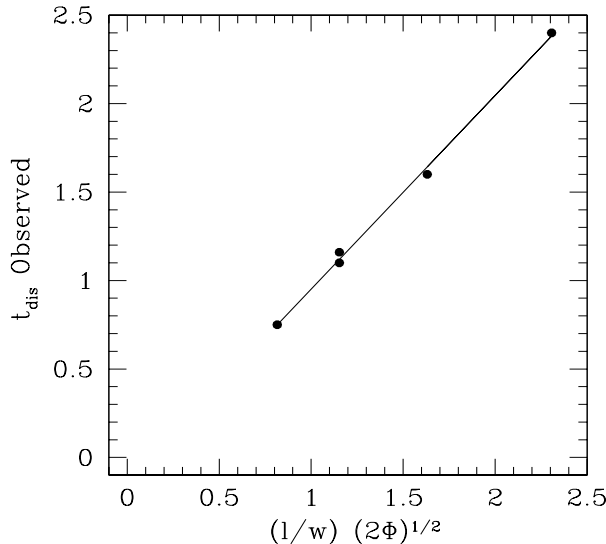


FIG. 6.— Determination of the effective drag coefficient for our clumps, from plotting estimated disruption times t_{dis} vs. the quantity $(l/w_g)(2\Phi)^{1/2}$; the slope is then $C_D^{-1/2}$. This determination is slightly qualitative as to when we judge the clump to be disrupted; we decided to use the time at which vortex-driven voids first appear in a $a-z$ planar cross-section through the nominal center of the clump.

$Re_c/2$ where Re_c is the Reynolds number of a clump, and we have approximated $dw_g/dr \sim w_g/(l/2)$. Because we are dominated by numerical viscosity, $\nu'_n \sim w'_g \Delta$, thus in code units $Re'_c \sim w'_g l' / 2w'_g \Delta = l' / 2\Delta \approx 5$ in many cases so far. For comparison, the Reynolds number for *nebula* clumps of interesting sizes is $> 10^6$. This means that viscous stresses around the periphery of the clump, and the fractional depth of the viscous boundary layer, are grossly exaggerated in the numerical model relative to the actual nebula regime of interest. The anomalously large role of (numerical) viscosity leads to anomalously large “erosion” from the surface of our numerical clumps, and degrades our results in the sense that potentially stable clumps *might* appear less stable, due to the erosive mass loss experienced over their sedimentation time. Going to higher resolution cases ($Re'_c \sim 10$) significantly ameliorated this effect but the problem has certainly not been entirely removed. Another way to characterize the degree of artificial erosion is to estimate the *physical* Kolmogorov scale for the actual nebula/clump situation: for $\nu = 10^6$ cm sec $^{-2}$, $l = 10^4$ km, and $w_g = 3800$ cm/s, we find $\eta \sim 100$ m, or 10^{-5} of the size of a 10^4 km clump, compared to a fractional size of perhaps 10^{-1} or so in the code, as determined by numerical viscosity. Clearly, surface erosion is a much smaller effect in the nebula case than in our crude models. While even at this resolution apparently stable configurations can be found, it would be desirable for future studies to improve on this situation.

Clump drag coefficient C_D : The drag coefficient of the clump is Reynolds-number-dependent and must also be scaled to nebula values to obtain an estimate of Φl . Weidenschilling (1977) gave expressions for the drag force per unit area (giving the pressure force per unit area), experienced by solid spheres of different Re_c in the Stokes drag regime of interest here, as $C_D \rho_g w_g^2 / 2$. For $1 < Re_c < 800$, $C_D = 24/Re_c^{0.6}$, or $C_D \sim 8$ for $Re_c \sim 5$, as in our code. The large drag coefficient and ram pressure is partly due to low-pressure zones set up immediately behind particles in this range of Re_c . By comparison, for a solid sphere with $Re_c > 800$ as under nebula conditions, $C_D = 0.44$. However, neither of these values might be entirely applicable to our clumps, which are not rigid spheres. In practice, we have determined C_D empirically from observed values of t_{dis} with self gravity turned off. Recalling that $t_{dis} = (l/w_g)(2\Phi/C_D)^{1/2}$, we simply plot our estimate of t_{dis} , the point at which sizeable vortex-driven internal voids appear in the clump, against the combined parameter $(l/w_g)(2\Phi)^{1/2}$, giving $C_D^{-1/2}$ as the slope of the best fit straight line (**figure 6**). It seems that $C_D \approx 1$ is a good assumption, but this calculation should be redone with higher resolution (lower numerical viscosity) codes. At nebula Re_c , C_D could reach its theoretical high- Re value of 0.4 and this is what we assume in deriving Φl .

Finally then, the several stable cases we have run (*eg.* figure 3) can be characterized by $w'_g = 38$ rad/ctu, $\rho'^* = 380$ (which corresponds to a minimum mass nebula local density $\rho_g = 10^{-10}$ at distance 2.5 AU), $\Phi = 10^3$, and $l' \approx 1$ radian, and while we have not as yet accurately determined the transition value of We_G , a value $We_G \sim 1$ is clearly stable. Solving equation (4) of section 3.3 for Φl under *nebula* conditions, *assuming* $We_G^* = 1$, taking $C_D = 0.44$ for a high- Re_c situation and assuming a nominal $\beta = 10^{-3}$, we find $\Phi l > 1.5 - 5 \times 10^6$, independent of ρ_g and neglecting a questionable coefficient of order unity (because of the contribution of viscous stresses in our low- Re_c code). Foreseeable refinements (specifically, lower numerical viscosity) may increase We_G^* (the surface tension analogue gives $We_G^* \sim 10$) and thus decrease the value of Φl .

APPENDIX C: TIME EVOLUTIONS AND MOVIES

Quicktime movies showing our time evolutions are available online at <http://spacescience.arc.nasa.gov/users/cuzzi/>,

with filenames as given below. After publication, the movie files will also be available on the ApJ web site as mp4s. Each shows a dense clump in the Hill frame, rotating at local Keplerian velocity, with more slowly-orbiting gas impinging on the clump from its leading side. The two left-hand panes show the view from along the radial axis (in the $Z - \theta$ plane; top) and along the vertical axis (in the $a - \theta$ plane; bottom). The large right-hand pane shows the view from the orbitally leading direction (in the $a - Z$ plane). The wake formed by the clump is easily visible in the two left-hand panes. Cases hill26.gif and hill29a.gif are sampled at a similar time near their end-point in figure 3. File hill26.gif shows how a clump with no self-gravity is disrupted in about 1.5 code time units for the initial conditions chosen (the orbit period is 2π code time units), in agreement with our simple estimates of t_{dis} . Files hill29a.gif and hill31a.gif are intended to illustrate the same (stable) Weber number case ($We_G \sim 1$) but we vary two constituent parameters of We_G (we decrease both the gas velocity and mass loading by a factor of three) to illustrate similarity; because of the specific parameters chosen, hill31a.gif runs for a longer time, but is suffering considerable erosion towards the end of the run. Nevertheless, as discussed below, it retains a dense core that continues to contract. As discussed in Appendix B, more realistic cases, with higher numerical resolution, would have smaller numerical viscosity and incur less erosion. Case hill29a.gif, while not run as long as hill31a.gif, appears solidly stable with a dense core that is continuing to shrink at the end of the run. Note some interesting oscillatory behavior, such as hinted at in our 1D compressible runs (figure 2).

Behavior of central regions of dense clumps

The simulations which created the movies referred to above can be used to assess the behavior of the central, dense regions of each clump in a quantitative manner. **Figure 7** has three panels, showing the time variation of some properties of the particles which lie within the central regions of the clump (its densest fraction, as sampled out to some cumulative mass threshold). In the top panel, we show how much mass is being eroded from the clump overall (particles moving faster than some comoving velocity threshold are assumed to have left the clump). All three clumps are losing mass, naturally, but the non-gravitating clump 26 is losing it much more rapidly than the gravitating clumps 29a and 31a. In the central panel we show the mean mass density as measured over some fraction f of the clump mass lying at the highest densities; in clumps 26 and 29a, we chose $f = 0.5$, and in clump 31a, we chose $f = 0.25$. In the non-gravitating clump, the core density never increases and it quickly blows up, while the central regions of the gravitating clumps (removed from the artificial mass erosion at their peripheries) inexorably get denser at a steady and perhaps even slightly increasing rate (an increasing rate is predicted by the simple model). The lower panel shows the effective average radius of the region being sampled. The non-gravitating clump never shrinks at all, but both gravitating clumps do. Moreover, as the gravitating clumps shrink, their density increases faster than their linear dimension decreases, so the product Φl increases - causing them to become *more* stable as time goes on. This is an argument for stability even in the presence of erosion. As expected, the density growth timescale (the sedimentation time t_{sed} of equation 1) is three times smaller for the denser clump of case 29a (middle panel). Meanwhile, the apparent agreement of the variation of the fractional radius containing half of the mass seen between cases 29a and 31a in the lower panel is fortuitous, because the total masses of the clumps are changing (and eroding) at different rates and from different depths in the two cases. Nevertheless, the cores are both shrinking and becoming denser in the two stable cases. The amount of erosion that is incurred from the margins of each clump is related to (perhaps proportional to) the thickness of the viscous boundary layer relative to the radius of the clump, which can be expressed in terms of the Reynolds number. As we have argued above in this Appendix, actual nebula clumps capable of remaining stable would have Reynolds numbers five orders of magnitude larger - impossible to study with numerical models. The relevance of all viscous boundary layer effects, including the erosion that inflicts our current numerical runs, will decrease by that factor in the real situation.

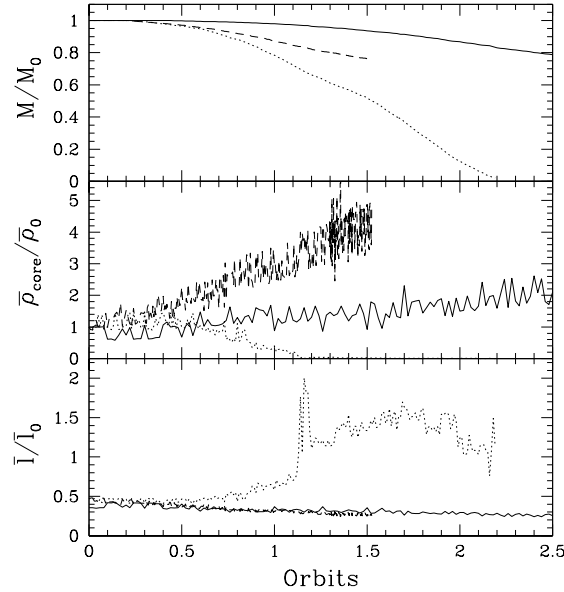


FIG. 7.— Properties of the dense central regions in three simulations, as a function of time. Cases are shown in each panel as: solid line (stable, self-gravitating case 31a); dashed line (stable, self-gravitating case 29a); and dotted line (unstable, non-gravitating case 26). Not all cases were run to the same stopping point due to resource constraints. Top: cumulative total mass retained by the clump; middle panel: average mass density of the central mass fraction f ; bottom panel: effective radius containing mass fraction f . These results show that, away from the artificially perturbed perimeter regions, We_G -stable clumps are behaving as expected by the simple model, and We_G -unstable clumps do not show this behavior.

REFERENCES

- Afshordi, N., Mukhopadhyay, B., and Narayan, R. 2005, *Astrophys. J.* 629, 373
- Ahmed, A. M., and Elghobashi, S. 2000, *Phys. Fluids* 12, 2906
- Ahmed, A. M., and Elghobashi, S. 2001, *Phys. Fluids* 13, 3346
- Arltdt, R. and Urpin, V. 2004, *Astron. Astrophys.* 426, 755
- Asphaug, E. and Benz, W. 1996, *Icarus*, 121, 225
- Balbus, S. A. Hawley, J. F. and Stone, J. M. 1996, *Astrophys. J.* 467, 76
- Bell, K. R., Lin, D. N. C., Hartmann, L. W., and Kenyon, S. J. 1995, *Astrophys. J.* 444, 376
- Binzel, R. P., Lupishko, D., DiMartino M., Whitely, R. J., and Hahn, G. J. 2002, in *Asteroids III*; W. F. Bottke, jr., A. Cellino, P. Paolicchi, and R. P. Binzel, eds; Univ. of Arizona Press
- Bischoff, A., Scott, E. R. D., Metzler, K., and Goodrich, C. A. 2006, in “Meteorites and the Early Solar System, II”; D. Lauretta and H. McSween, eds.; Univ. of Arizona Press; 679
- Bosse, T., L. Kleiser, and E. Meiburg 2006, *Phys. Fluids* 18, paper id 027102
- Bottke, W. F. jr., Durda, D. D., Nesvorny, D., Jedicke, R., Morbidelli, A., Vokrouhlicky, D., and Levison, H. 2005, *Icarus*, 175, 111
- Brearley, A. J. 1993, *Geochim. Cosmochim. Acta* 57, 1521-1550
- Brownlee, D. P. and 1001 authors, 2006, *Science* 314, 1711
- Busse, F. 2004, *Science* 305, 1574
- Canuto, C., Hussaini, M.Y., Quarteroni, A., and Zang, T.A 1987, “Spectral Methods in Fluid Dynamics”, Springer-Verlag, New York
- Chambers, J. E. 2004, *E. P. S. L.* 223, 241
- Chambers, J. E. 2006, in “Meteorites and the Early Solar System, II”; D. Lauretta and H. McSween, eds.; Univ. of Arizona Press, 487
- Ciesla, F. J. 2007, *Science* 318, 613
- Ciesla, F. J. and Cuzzi, J. N. 2006, *Icarus*, 181, 178
- Connolly, H. C., Desch, S. J., Ash, R. D., and Jones, R. H. 2006, in “Meteorites and the Early Solar System, II”; D. Lauretta and H. McSween, eds.; Univ. of Arizona Press; 383
- Cuzzi, J. N. and Alexander, C. M. O’D. 2006, *Nature*, 441, 483
- Cuzzi, J. N., Davis, S. S., and Dobrovolskis, A. R. 2003, *Icarus*, 166, 385
- Cuzzi, J. N., Ciesla, F. J.; Petaev, M. I.; Krot, A. N.; Scott, E. R. D.; and Weidenschilling, S. J. 2005, in “Chondrites and the Protoplanetary Disk”, A.S.P. Conf. Ser., 341, 732
- Cuzzi, J. N., Dobrovolskis, A. R., and Champney J. M. 1993, *Icarus*, 106, 102
- Cuzzi, J. N., Hogan, R. C., Paque, J. M., and Dobrovolskis, A. R. 2001, *Astrophys. J.*, 546, 496
- Cuzzi, J. N., Hogan, R. C. and Shariff, K. 2007, 38th LPSC, paper 1439
- Cuzzi, J. N. and Weidenschilling, S. J. 2006, in “Meteorites and the Early Solar System, II”; D. Lauretta and H. McSween, eds.; 353
- D’Alessio, Calvet, P., N., and Woolum, D. S. (2005) A.S.P. Conference Series, 341, 353
- Desch, S. J., Ciesla, F. J., Hood, L. L., and Nakamoto, T. 2005, A.S.P. Conf. Ser., 341, 872
- Dodd, R. T. 1976, *Earth and Plan. Sci. Lett.* 30, 281
- Dominik, C. P., Blum, J., Cuzzi, J. N., and Wurm, G. 2007, in “Protostars and Planets V”, Univ. of Az. Press, B. Reipurth, S. Krot, and E. R. D. Scott, eds., p. 783
- Dubrulle, B., G. E. Morfill, and M. Sterzik 1995, *Icarus* 114, 237
- Dubrulle, B., Marie, L., Normand, Ch., Richard, D., Hersant, F., and Zahn, J.-P. 2005, *Astron. Astrophys.* 429, 1
- Dullemond, C. P. and Dominik, C. 2005, *Astron. Astrophys.* 434, 971
- Eaton, J. and Fessler, J. R. 1994, *Int. J. Multiphase Flow*, 20, Suppl. 169
- Falkovich, G. and Sreenivasan, K. R. 2006, *Physics Today* 59, 43
- Gaffey, M. J., Bell, J. F., Brown, R. H., Burbine, T. H., Piatek, J. L., Reed, K. L., and Chaky, D. A. 1993, *Icarus*, 106, 573
- Gaffey, M. J., Cloutis, E. A., Kelley, M.S., and Reed, K. L. 2002, in *Asteroids III*; W. F. Bottke, jr., A. Cellino, P. Paolicchi, and R. P. Binzel, eds; Univ. of Az. Press, p. 183
- Garaud, P. and Lin, D. N. C. 2004, *Astrophys. J.* 608, 1050
- Ghosh, A., Weidenschilling, S. J., McSween, H. Y. jr., and Rubin, A. 2006, in “Meteorites and the Early Solar System, II”; D. Lauretta and H. McSween, eds.; 555
- Goldreich, P. and Lynden-Bell, D. 1965, *Mon. Not. Roy. Ast. Soc.* 130, 97
- Goldreich, P. and Ward, W. R. 1973, *Astrophys. J.* 183, 1051

- Grimm, R. E., Bottke, W. F., Durda, D., Scott, E. R. D., Asphaug, E., and Richardson, D. 2005, 36th LPSC, League City, Texas, Abstract 1798.
- Grossman, J. N. 1988, in "Meteorites and the Early Solar System", J. F. Kerridge and M. S. Matthews, eds, Univ. of Az. Press, 680
- Grossman, J. N., Rubin, A. E., Nagahara, H., and King, E. A. 1988, in "Meteorites and the Early Solar System", J. F. Kerridge and M. S. Matthews, eds, Univ. of Az. Press, 619
- Haghighipour, N. and Boss, A. P. 2003, *Astrophys. J.* 598, 1301
- Hevey, P. J. and Sanders, I. S. 2006, *Meteoritics Plan. Sci.* 41, 95
- Hogan, R. C. and Cuzzi J. N. 2001, *Phys. Fluids*, 13, 2938
- Hogan, R. C. and Cuzzi J. N. 2007, *Phys. Rev. E.*, 75, paper id 056305
- Hughes, D. W. 1978, *Earth Pl. Sci. Lett* 38, 391
- Hughes, D. W. 1980, *Earth Pl. Sci. Lett* 51, 26
- Johansen, A., Klahr, H., and Henning, Th. 2006, *Astrophys. J.* 636, 1121
- Johansen, A., Oishi, J. S., MacLow, M.-M., Klahr, V., Henning, Th., and Youdin, A. 2007, *Nature* 448, 1022
- Jones, R. H., Lee, T., Connolly, H. C. jr., Love, S. G., and Shang, H. 2000, in "Protostars and Planets IV", eds. V. Mannings, A. P. Boss, and S. S. Russell, Univ. of Ariz. Press, 927.
- Jones, R. H., Grossman, J. N., and Rubin, A. E. 2005, in A.S.P. Conference Series 341, 251
- Juneja, A., Lathrop, D. P., Sreenivasan, K. R. and Stolovitsky, G. 1994, *Phys. Rev. E.*, 49, 5179
- Kenyon, S. J. and Bromley, B. C. 2004, *Astrophys. J.* 127, 513
- Kenyon, S. J. and Bromley, B. C. 2006, *Astrophys. J.* 131, 1837
- Kita, N. T., Huss, G. R., Tachibana, S., Amelin, Y., Nyquist, L. E., and Hutcheon, I. D. 2005, ASP Conference Series 341, 558
- Klahr, H. H. and Bodenheimer, P. 2003, *Astrophys. J.* 582, 869
- Kleine, T., Metzger, K., Palme, H., Scherer, E., and Münker, C. 2005, *Geochim. Cosmochim. Acta* 69, 5805
- Kleine, T., Halliday, A. N., Palme, H., Metzger, K., and Markowski, A. 2006, 37th LPSC, League City, Texas; Abstract 1884
- Langkowsky, D., Teiser, J., and Blum, J. 2007, *ApJ*, in review, arXiv:0711.2148
- LaTourrette, T., and Wasserburg, G. J. 1998, *Earth Planet. Sci. Lett.*, 158, 91
- McSween, H. Y., Ghosh, A., Grimm, R. E., Wilson, L., and Young, E. D. 2002, in *Asteroids III*; W. F. Bottke, jr., A. Cellino, P. Paolicchi, and R. P. Binzel, eds; Univ. of Ariz. Press
- Meneveau, C. and Sreenivasan, K. R. 1991, *J. Fluid Mech.* 224, 429
- Metzler, K., Bischoff, A. and Stöffler, D. 1992, *Geochim. Cosmochim. Acta* 56, 2873
- Moskovitz, N. A., Millman, M., Lawrence, S. J., Jedicke, R., Nesvorný, D., and Gaidos, E. J. 2007, 38th LPSC, League City, Texas; paper 1663
- Mukhopadhyay, B. 2006, *Astrophys. J.* 653, 503
- Mukhopadhyay, B., Afshordi, N., and Narayan, R. 2005, *Astrophys. J.* 629, 383
- Nakagawa, Y., Sekiya, M., and Hayashi, C. 1986, *Icarus*, 67, 375
- Ormel, C. W., Cuzzi, J. N., and Tielens, A. G. G. M. 2008, *ApJ*, in review
- Paque, J. M. and Cuzzi, J. N. 1997, 28th LPSC, p. 1071
- Petit, J.-M., Morbidelli, A., and Chambers, J. E. 2001, *Icarus* 153, 338
- Pruppacher, H. R., and Klett, J. D. 1997, *Microphysics of clouds and precipitation*; Kluwer Academic
- Rice, W. K. M., Lodato, G., Pringle, J. E., Armitage, P. J., and Bonnell, I. A. 2004, *Mon. Not. Roy. Ast. Soc.* 355, 433
- Russell, S. S., Hartmann, L. A., Cuzzi, J. N., Krot, A. N., and Weidenschilling, S. J. 2006 in "Meteorites and the Early Solar System, II"; D. Lauretta and H. McSween, eds.; 233
- Sirono, S.-I. 2000, *Icarus* 167, 431
- Safronov, V. 1991, *Icarus*, 94, 260
- Scott, E. R. D. 2006, *Icarus* 185, 72
- Scott, E. R. D. and Krot A. N. 2005, in A.S.P. Conf. Series 341, 15
- Sekiya, M. 1983, *Prog. Theor. Physics*, 69, 1116
- Sekiya, M. 1998, *Icarus* 133, 298
- Sekiya, M. and Ishitsu, N. 2001, *Earth, Planets, and Space* 53, 761
- Sekiya, M. and Takeda, H. 2003, *Earth, Planets, and Space* 55, 263
- Skinner, W. R., and Leenhouts, J. R. 1993, LPSC XXIV, 1315
- Squires, K. R. 1990, PhD thesis, Stanford University
- Squires, K. and Eaton, J. K. 1990, *Phys. Fluids* A2, 1191
- Squires, K. and Eaton, J. K. 1991, *Phys. Fluids* A3, 1169
- Sreenivasan, K. R. and Stolovitsky, G. 1995, *J. Stat. Physics* 78, 311
- Stone, J. M.; Gammie, C. F., Balbus, S. A., and Hawley, J. F. 2000, in *Protostars and Planets IV*; V. Mannings, A. P. Boss, and S. S. Russell, eds. Univ. of Az. Press; 589
- Taylor, G. J., Maggiore, P., Scott, E. R. D., Rubin, A. E., Huss, G. R., and Keil, K. R. 1987, *Icarus* 69, 1
- Taylor, S. R. (2005) *Solar System Evolution: a new perspective*; Cambridge (2nd ed.)
- Tennekes, H., and Lumley, J. L. 1972, *A First Course in Turbulence*, MIT Press, Cambridge Mass.
- Thomson, J. J., and Newhall, H. F. 1885, *Proc. Roy. Soc.* 39, 417
- Toomre, A. 1964, *Astrophys. J.* 139, 1217
- Trieloff, M., Jessberger, E. K., Herrwerth, I., Hopp, J., Fiéni, C., Ghéllis, M., Bourrot-Denis, M., and Pellas, P. 2003, *Nature*, 422, 502
- Turner, N. J., Sano, T., and Dziourkevitch, N. 2007, *Astrophys. J.* 659, 729
- Umurhan, O. M. and Regev, O. 2004, *Astron. Astrophys.* 427, 855
- Wadhwa, M., Y. Amelin, A. M. Davis, G. W. Lugmair, B. Meyer, M. Gounelle, and S. J. Desch 2007, in "Protostars and Planets V", B. Reipurth, D. Jewitt, and K. Keil, eds; Univ. of Az. Press, p. 835
- Weidenschilling, S. J. 1980, *Icarus* 44, 172
- Weidenschilling, S. J. 2000, *Space Sci. Revs.* 92, 295
- Weidenschilling, S. J. and Cuzzi, J. N. 2006, in "Meteorites and the Early Solar System, II"; D. Lauretta and H. McSween, eds.; 473
- Weisberg, M. K., McCoy, T. J., and Krot, A. N. 2006, in "Meteorites and the Early Solar System, II"; D. Lauretta and H. McSween, eds.; 19
- Woolum, D., and Cassen, P. M. 1999, *Meteoritics and Planetary Science*, 34, 897
- Youdin, A. and Shu, F. H. 2002, *Astrophys. J.* 580, 494
- Youdin, A. and Chiang, E. 2004, *Astrophys. J.* 601, 1109
- Zolensky, M. and 1001 authors 2006, *Science* 314, 1735